PEER REVIEWED

Environmental, Economical, and Performance Impacts of Ar-H$_2$ and N$_2$-H$_2$ Plasma-Sprayed YSZ TBCs

Rogerio S. Lima[1] · Bruno M. H. Guerreiro[1] · Nicholas Curry[2] · Matthias Leitner[2] · Karl Körner[2]

Abstract Since the 1970s, the Ar-H$_2$ plasma has been the standard air plasma spray (APS) gas system employed to deposit ZrO$_2$-Y$_2$O$_3$ (YSZ) thermal barrier coatings (TBCs) for the gas turbine industry, particularly regarding the legacy plasma spray torches. Although much less costly and yielding higher YSZ deposition efficiency (DE) levels, N$_2$-H$_2$ plasmas did not become the mainstream plasma system. This N$_2$-H$_2$ issue likely occurred due to problems like preliminary APS torch Cu-nozzle erosion (Cu contamination on TBCs) and the tendency to produce denser coatings, potentially leading to TBCs exhibiting higher thermal conductivity (TC) and lower thermal cycle lifetimes. However, in the twenty-first century, environmental footprint reduction and economical aspects are becoming paramount. In addition, the introduction of new technologies (e.g., tungsten-lined Cu nozzles, particle T&V sensors, and computer-controlled automation) has dramatically increased the stability and reproducibility of APS processing. Therefore, the N$_2$-H$_2$ plasma concept needs to be revisited with respect to the legacy plasma spray torches, which are still highly used by the gas turbine industry original engine manufacturers and service centers worldwide. In this paper, different sets of APS YSZ TBCs were deposited via Ar/H$_2$ and N$_2$/H$_2$ plasmas using the legacy 3MB APS torch. The DE, TC, and furnace cycle test (FCT) were evaluated. The best FCT-performing Ar-H$_2$ and N$_2$-H$_2$ TBCs exhibited equivalent lifetimes. Moreover, the best FCT-performing N$_2$-H$_2$ TBC demonstrated a 100% increase in DE and an overall 55% reduction in production cost when compared to the best FCT-performing Ar-H$_2$ TBC. Finally, the TC values at room temperature and 1200 °C of best FCT-performing N$_2$-H$_2$ TBC were within the range of those of Ar-H$_2$ TBCs.

Keywords APS · Ar-H$_2$ · deposition efficiency (DE) · environmental footprint · N$_2$-H$_2$ · TBC · thermal conductivity · thermal cycling (FCT) · YSZ

Introduction

Thermal Barrier Coatings (TBCs) Manufactured via Air Plasma Spray (APS)

TBCs manufactured via APS provide thermal insulation from the hot combustion gas stream to the metallic parts located in the hot sections of gas turbine engines (e.g., combustion chambers) (Ref 1). A thermally sprayed TBC system typically exhibits a bilayered structure, which includes a ceramic topcoat and a metallic MCrAlY (M = Ni, Co. NiCo or CoNi) bond coat (BC) (Ref 1). The ceramic topcoat (e.g., ZrO$_2$-7-8 wt.%Y$_2$O$_3$, a.k.a., YSZ) provides thermal insulation and reduces the heat flow to the turbine metallic part. The metallic BC is an oxidation-/corrosion-resistant metallic layer. It protects the underlying component and improves the adhesion of the ceramic topcoat on the part.

✉ Rogerio S. Lima
rogerio.lima@cnrc-nrc.gc.ca

[1] National Research Council of Canada, 75 de Mortagne Blvd., Boucherville, QC J4B 6Y4, Canada

[2] Treibacher Industrie AG, Auer-von-Welsbach-Straße 1, 9330 Althofen, Austria

## Ar-Based and N₂-Based Plasmas: Key Differences

Briefly, it is important to highlight that plasma is a "cloud" of an ionized gas formed by positive ions and free electrons. To create a plasma in APS torches, an initially non-ionized gas (e.g., Ar or N_2) flows in between the cathode and anode (i.e., electrodes). Subsequently, an electric field (i.e., voltage) is applied between the electrodes. When the breakdown voltage is achieved (i.e., energy input), a current can be maintained as the free electrons and ions move along the ionized gas. As the plasma gas propagates throughout the torch nozzle to the ambient away from the energy input, the electrons and ions recombine, thereby releasing energy in the form of heat and light. Specifically regarding APS torches, Ingham Jr. and Fabel (Ref 2) discussed some of the key differences between Ar-based and N_2-based plasmas on how powder particles are melted during spraying. Figure 1 shows the enthalpy (i.e., total heat content) of main APS torch gases *versus* gas temperatures values (Ref 2).

Monoatomic gases like Ar undergo ionization and subsequent deionization. Diatomic gases like N_2 undergo dissociation, followed by ionization and subsequent deionization and recombination. From Fig. 1, it can be inferred that the N_2 plasma achieves electrical conductivity to sustain thermal plasma at temperatures below 10,000 K ($\sim$ 10,000 °C). For Ar, the electrical conductivity to sustain thermal plasma begins at temperatures higher than 10,000 K (i.e., when the Ar enthalpy shows a sudden steep increase). Therefore, N_2 becomes an effective plasma gas for melting powder particles because of the high heat content (i.e., enthalpy) available. Regarding Ar, it becomes an effective heating plasma gas for melting powder particles because of its high temperature level.

Moreover, Murphy and Arundell (Ref 3) showed that the thermal conductivity of an Ar plasma at temperatures of 10,000-17,000 K (Fig. 1) reaches a maximum of $\sim$ 2.5 W/mK. However, that of N_2 plasma reaches a maximum of $\sim$ 5.5 W/mK at temperatures of 5000-10,000 K (Ref 3). Therefore, from Fig. 1, it is noticed that at the peak of their respective thermal performances, the N_2 plasma exhibits essentially twice the thermal conductivity of the Ar plasma. For this reason, the higher thermal conductivity levels of the N_2 plasma will improve its capability to melt thermally sprayed particles, at least when compared to the Ar one.

Another important factor on the capability to melt powder particles during APS deposition is the plasma velocity (Ref 2). The plasma velocity controls the dwell time of the powder particles in the plasma plume during spraying. The temperatures shown in Fig. 1 allow a discussion of plasma velocity levels. Initially, it is necessary to consider the ideal gas law $V = (nRT)/P$; where V = gas volume, n = number of moles, R = gas constant, T = gas temperature, and P = gas pressure. The velocity of a plasma plume is primarily caused by the rapid volume expansion resulting from the temperature to which the gas is heated by the torch. Figure 1 shows that Ar plasma temperatures are higher than those of N_2 plasmas. For this reason, the velocities of Ar-based plasmas will tend to be higher than those of N_2-based ones. As the velocity of the powder particles is proportional to the velocity of the plasma gas (via dragging), N_2-based plasma-sprayed particles will tend to exhibit lower velocity levels than those sprayed via Ar-based plasmas (under similar conditions of power, flow and spray distance). The combinations of these gases produce different particle melting conditions via plasma enthalpy, plasma temperature, plasma thermal

Fig. 1 Plasma temperature as a function of gas energy content at atmospheric pressure (from Ref 2)
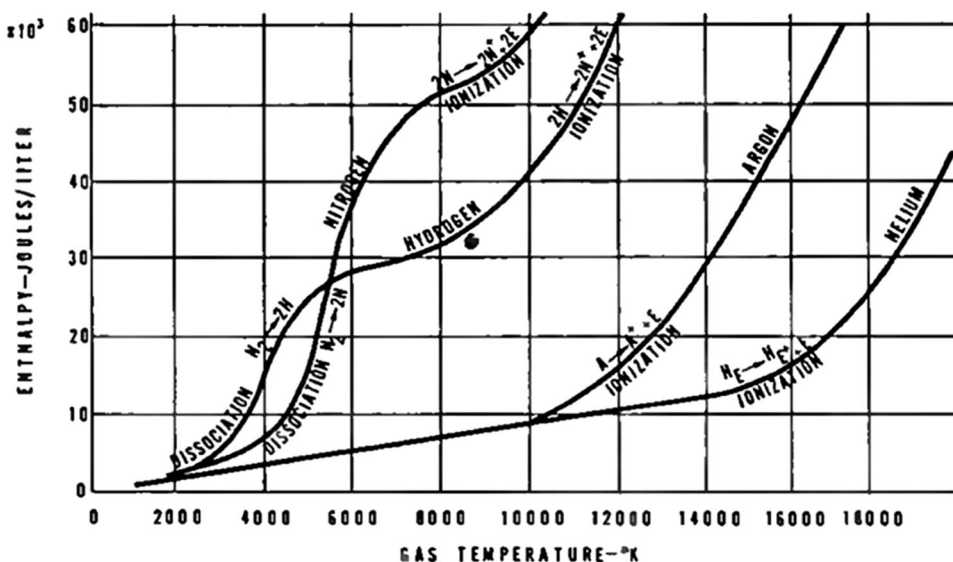
conductivity, plasma velocity, and particle dwell time in the plasma plume.

Marple et al. (Ref 4) looked at this issue into more detail. A commercially available plasma-spheroidized YSZ TBC powder was sprayed via a legacy APS torch (Metco 9MB). Using different spray parameters but under similar conditions of power and flow, a total of 10 and 12 YSZ TBCs were sprayed via Ar-H_2 and N_2-H_2 plasmas, respectively. The summary of the results is given in Table 1. Consequently, the study of Marple et al. (Ref 4) corroborates the findings of previous works (Ref 2, 3). It shows that Ar-based plasmas tend to induce higher particle velocities and lower particle temperatures when compared to N_2-based ones (under similar conditions of power, flow, and spray distance). This study also shows the important advantage of using N_2-H_2 plasmas in order to increase the deposition efficiency of YSZ powders for TBC production, which will be discussed in this manuscript.

On a final note, it needs to be stated that the H_2 and helium (He) typically employed as a secondary gas for the legacy APS torches, have the practical effect of increasing the thermal conductivity (i.e., thermal efficiency) of the Ar and N_2 primary plasmas (Ref 2). However, they do not significantly affect the fundamental heating and momentum of the primary gas. Due to its high cost, helium is now being avoided by the industry.

Ar-Based and N_2-Based Plasmas Perspectives on TBCs

Legacy APS torches (e.g., 3MB, 9MB, F4 and variations of these) were the main ones commercially available for the gas turbine industry when TBCs came to be implemented during the mid-1970s and 1980s. At that time, plasma gas flow and current were set by manually adjusting (via human eye) rotameters and knobs. The flow of plasma gases, torch power, and torch cooling were not recorded during spraying. There were no commercial sensors to measure thermal spray particle temperature and velocity and APS copper nozzles without tungsten lining were the only ones available. Consequently, it is easy to imagine that the thermal spray processing 40 years ago lacked reliability and reproducibility. Under these circumstances, the initial parameter sets and specs for TBCs were written.

As previously shown in Table 1, N_2-H_2 plasmas can induce much higher deposition efficiency levels than those of Ar-H_2 plasmas. In spite of that, the authors of this manuscript did not find any official reference on why Ar-H_2 plasmas were preferred over the N_2-H_2 ones for the legacy APS torches (regarding the early TBC specs). Nonetheless, by "anecdotal evidence" (i.e., informal statements from members of the thermal spray community), it seems that Ar/H_2 plasma was preferred mainly due to its lower probability of eroding the copper nozzles (anodes) of the torches, thereby minimizing the potential of copper spiting and contamination on the TBC structure. El-Zein et al. (Ref 5) have shown that under similar gas flow levels, the current density (A/cm^2) of a N_2 plasma is $\sim 25\%$ higher than that of an Ar one. Higher current density is linked to higher heat load of the anode (nozzle) wall and thus its erosion. At the same time, once a process is set and specs are written, it is expensive to change and qualify new processes and write new specs, particularly for the gas turbine industry. For this reason, YSZ TBCs sprayed via Ar-H_2 plasmas still remain as the mainstream plasma system for legacy APS torches for the last 40 years.

Environment, Economics, and Reality in the Twenty-First Century

The twenty-first century is bringing a revolution in terms of environment, economics, and data. The environmental laws are getting tougher and companies are facing a stiffer competition to improve the quality of their products without causing more harm to the ambiance and climate. Higher demand for increasing productivity with a reduction in cost and environmental footprint is paramount.

According to Sampath et al. (Ref 6), in 2011 approximately 1-1.5 million kg of YSZ were deposited onto engine components via APS. Considering that the majority of this material was sprayed via legacy torches (i.e., Ar-H_2 plasma), we can assume that at least 50% of the sprayed YSZ was not deposited on the components due to low DE levels. In other words, at least 0.5-0.75 million kg of YSZ was lost in dust collectors and ventilation systems at that year. In addition, it is important to highlight the lost YSZ powder cannot be recycled for further thermal spray applications. Moreover, attempts to recycle thermal spray

Table 1 Summary of the particle temperature, velocity, spray distance, and deposition efficiency values for Ar/H_2 and N_2/H_2 plasmas for YSZ using a 9MB APS torch (Ref 4)

Plasma	Particle temperature range, °C	Particle velocity range, m/s	Spray distance range, cm	YSZ deposition efficiency (DE) range, %
Ar/H_2	2500-2780	130-160	11-17	10-38
N_2/H_2	2550-3100	70-120	11-17	5-70

ceramic powders caught up in dust collectors to other applications have been "timid" at best. These numbers seem to be unrealistic under the reality that our society lives today. For this reason, it is thought that deposition efficiency values lower than 50% may no longer be accepted in the near future by the industry.

Today in modern processing systems, APS torches are computer-controlled, even the legacy ones. Plasma gases are set and fixed constant by mass-flow meters. The same concept applies to plasma current and power. Torch cooling is also monitored. Tungsten-lined copper nozzles for highly employed legacy APS torches like 3MB and 9MB are now available. The tungsten-lined nozzles provide higher processing security against TBC contamination during spraying and improve the longevity of the nozzle. In contrast with the past, different commercially available sensors are now readily available, which includes (1) sensors to measure particle temperature and velocity, (2) plasma plume characteristics, (3) infrared and high-speed cameras, and (4) even sensors to measure plasma spray sound/noise which are a reality. All these sets of data have the potential to be recorded, integrated and even analyzed in real-time using "big data" and the internet of things (IoT); a.k.a., Industry 4.0. Thus, nowadays, processing adjustments can be rapidly addressed or equipment malfunctions can be more easily detected before spraying is performed.

Rationale and Objectives

Based on the facts above cited, it is worth starting a detailed study on the comparison of both Ar-H_2 and N_2-H_2 plasmas using a legacy APS torch for TBC production. Although newer APS torch technologies are now available in the market (e.g., cascade plasma torches), based on random comments of members of the thermal spray community, it is estimated that about 90% of all APS torches employed in the world at this moment are the "legacy ones." Therefore, as the majority of these legacy torches have the option to work with N_2 as the primary plasma gas, the potential economic impact of this study is evident.

For this reason, the goal of using a N_2-H_2 plasma is to minimize cost by increasing YSZ deposition efficiency, while meeting the requirements of the application. Conventional wisdom would claim that N_2-H_2 plasma YSZ TBCs will be "too dense," thereby yielding:

(a)   High thermal conductivity and low thermal barrier effectiveness;

(b)   High stiffness and low capability to accommodate stress/strain;

(c)   Low performance in thermal cycle life.

The objective of this initial work is to show that N_2-H_2 plasma YSZ TBCs produced via a legacy APS torch can be engineered to exhibit significantly higher deposition efficiency levels than those of a Ar-H_2 plasma, while meeting the key performance standards (i.e., thermal conductivity and thermal cycle life) of Ar-H_2 plasma YSZ TBCs.

Experimental Procedure

TBC Production Using Ar-H_2 and N_2-H_2 Plasmas

All TBCs produced for this study (including top and bond coats) were sprayed using a single legacy APS torch (3MB, Oerlikon Metco, Westbury, NY, USA) for both Ar-H_2 and N_2-H_2 plasmas. It is important to highlight that all nozzles exhibited tungsten (W) lining and both the nozzles and cathodes were thorium (Th) free. Moreover, a mass-flow based computer-controlled console was employed to manage the TBC deposition. Table 2 shows some specific torch parts employed in this study.

The BC feedstock composition was NiCoCrAlY+HfSi (Amdry 386-4, Oerlikon Metco, Westbury, NY, USA). This powder displays a nominal particle size distribution of − 90/+ 38 μm. The BC was sprayed using a N_2-pure plasma (i.e., without H_2) at a spray distance (SD) of 7.5 cm using a carrousel fixture (sample tangential speed of 110 cm/s and torch transverse speed of 1 mm/s). The substrates were grit-blasted with white Al_2O_3 grit #60 prior to BC spraying. The BC thickness was 150-200 μm and its R_a roughness was 4.36 ± 0.56 μm (n = 10) (NRC ID#180417B2). It needs to be stressed that just one set of BC was employed for all Ar-H_2 and N_2-H_2 samples of this study.

The topcoat feedstock was ZrO_2-8 wt.%Y_2O_3 (Auer-Coat YSZ LD-A, Treibacher Industrie AG, Althofen, Austria). This powder shows an agglomerated and sintered (A&S) morphology, though unlike conventional powders, is manufactured from fine YSZ particles rather than a mixture of ZrO_2 and Y_2O_3 particles The powder had a nominal particle size distribution of d_{10}: 21 μm, d_{50}: 54 μm, and d_{90}: 97 μm. The YSZ TBC thickness was 400-450 μm for overall testing and characterization of this study, which includes: (1) microstructural characterization (metallography), (2) x-ray diffraction, (3) furnace cycle testing, and (4) instrumented indentation testing. The summary of the spray parameters employed to spray the YSZ is given in Table 3.

Moreover, in order to improve the accuracy and precision of this study, all YSZ TBCs employed in the overall testing and characterization above cited were produced in a single run using a carrousel fixture (sample tangential speed of 110 cm/s and torch transverse speed of 1 mm/s).

Table 2 Summary of nozzles, cathodes, and powder ports employed in this study for the Metco 3MB APS torch

Plasma	Nozzle (a)	Cathode (a)	Plasma injector ring (a)	Powder port (a)
Ar/H₂	GHW-TF	2M11-TF	3M275	#2 (1.85 mm)—dual
N₂/H₂	GW-TF	2M11-TF	3MBTD48979	#2 (1.85 mm)—dual

(a) Original (i.e., not generic) torch parts

Table 3 Summary of the spray parameters for YSZ deposition via 3MB APS torch

Set	NRC ID#	Ar flow, lpm	N₂ flow, lpm	H₂ flow, lpm	Powder feed rate, g/min	Carrier gas flow, lpm	Spray distance, cm	I, A	V (V)@power supply	P, kW
Ar-1	180419B1	50	n.a.	10	22	6 (Ar)	7.5	540	70	38
Ar-2	180420B2	50	n.a.	10	22	6 (Ar)	7.5	510	70	36
Ar-3	180423B1	50	n.a.	10	22	6 (Ar)	7.5	560	70	39
N₂-1	180417B3	n.a.	50	10	22	6 (N₂)	7.5	420	78	33
N₂-2	180418B1	n.a.	50	10	22	6 (N₂)	7.5	470	79	37
N₂-3	180418B3	n.a.	50	10	22	6 (N₂)	7.5	370	78	29

n.a.—not applicable

Nonetheless, the YSZ TBCs produced for deposition efficiency, density and thermal diffusivity/conductivity evaluation exhibited a thickness of 700-900 μm. They were initially sprayed together with the samples for overall testing and characterization (400-450 μm). However, to reach a thickness of 700-900 μm, a second spray run was performed immediately after.

The particle temperature (T) and velocity (V) values were measured using an infrared-based sensor (AccuraSpray G3C, Tecnar, St-Bruno, QC, Canada) at the same SD employed to produce the samples, i.e., 7.5 cm.

Microstructural Characterization

In order to better preserve their real microstructures, the as-sprayed and thermally cycled TBC samples were initially vacuum impregnated in epoxy resin and posteriorly ground/polished according to standard metallography procedures for TBCs. The cross-sectional microstructural features of the TBCs were analyzed by scanning electron microscopy (SEM).

X-ray Diffraction (XRD)

XRD using CuKα radiation was employed to evaluate the phase compositions of the as-sprayed YSZ TBCs. The XRD 2θ values ranged from 20° to 80° (scanning step size of 0.05° and step time of 2.5 s).

Deposition Efficiency (DE)

The YSZ TBCs employed to calculate DE values were sprayed onto white Al_2O_3 grit-blasted Almen N strips

(76.2 mm × 19.05 mm × 0.79 mm) without BC. The Almen N strips were placed together in the carrousel fixture along the other samples produced for this study. The DE was measured based on the weight of the strips before and after TBC deposition, as well as, on the powder feed rate and on the total time the torch was over the strip during spraying.

Instrumented Indentation Testing (IIT)

IIT (G200, Agilent Technologies, Santa Clara, CA, USA), a.k.a., depth-sensing indentation, was employed to measure the elastic modulus (E) values of the as-sprayed and thermal cycled (after failure) YSZ TBCs. This is the technique developed by Oliver and Pharr (Ref [7]), where the mechanical properties of materials can be determined directly from the indentation load and indentation displacement using high-resolution testing equipment. The E values (average of 10-12 indentations) were measured over the polished cross-sections of the coatings prepared for SEM evaluation (as described above) at RT. The IIT system employed a Berkovich indenter. The test was performed by using these main equipment setup inputs: YSZ Poisson's ratio estimated at 0.25, time to load 15 s, maximum indentation load of 300 gf and hold time at maximum indentation load of 10 s. Before testing the samples, the calibration of the equipment was double-checked with a fused silica (SiO_2) standard, using the same indentation setup inputs. A total of six indentations were generated before each TBC was probed. An average E value of $\sim$ 69 GPa was obtained, which is close to the results reported in the literature for SiO_2, i.e., $\sim$ 70 GPa (Ref [7]).

YSZ TBC Density and Porosity Measurements

The density of the YSZ TBCs was measured via the Archimedes water immersion technique. A total of eight free-standing coatings, prepared for thermal diffusivity/conductivity measurements (700-900 μm), were used to determine the density values for each YSZ TBC set. The YSZ TBCs were deposited on white Al_2O_3 grit-blasted low-carbon-steel substrates without BC. The samples were cut into 10 mm × 10 mm coupons using a precision sectioning saw. Subsequently, free-standing coatings were obtained by placing the coupons in an acid bath of hydrochloric acid, which dissolved the metallic substrate. The porosity was calculated based on the difference between the YSZ TBC density versus the density of a completely dense bulk YSZ sample.

Thermal Conductivity (TC) Measurements

Initially, the thermal diffusivity (TD) values of free-standing YSZ TBC coupons described above (700-900 μm) were measured using the Xenon lamp flash technique (HT HyperFlash, Netzsch GmbH, Germany). A total of four as-sprayed YSZ TBCs (for each spray set) were measured from room temperature (RT) up to 1200 °C in 200 °C temperature steps. The measurement steps consisted of five "shots" performed on each sample at each temperature step. Subsequently, three additional YSZ TBCs of each spray set were heat-treated in air at 1200 °C for 10 h, and additional three YSZ TBCs of each spray set were heat-treated in air at 1400 °C for 20 h. These heat treatments were performed to guarantee that the YSZ TBC microstructures would remain nearly stable prior to TD measurements at the high temperature levels (i.e., 1200 °C). These heat treatments induce sintering and aging of the samples.

The specific heat (Cp) of YSZ was measured by differential scanning calorimetry (STA 449 F3 Jupiter, Netzsch GmbH, Germany) in accordance with DIN Norm 51007 from room temperature up to 1250 °C. A sample of free-standing plasma-sprayed YSZ coating was used for analysis after heat treatment to 1450 °C. The plasma-sprayed coating is utilized for analysis, as it is a representative sample, having experienced the rapid heating and cooling from the coating process. However, a short heat treatment was performed to stabilize the sample structure and remove the influence of sintering that would otherwise influence the measurement, as pointed out by Di Girolamo et al. (Ref 8). The Cp values measured closely correlated to those reported by Taylor et al. (Ref 9). Finally, the TC values of the YSZ TBCs were calculated using the YSZ TBC density (d) values, the YSZ Cp values, and the YSZ TBC TD values; i.e., TC = d × Cp × TD. Evaluation of

the TC was carried out using Proteus thermal analysis software (Netzsch GmbH, Germany) using model correction for translucent materials.

Thermal Cycle Life: Furnace Cycle Testing (FCT)

For each spray set, a total of four TBCs were employed during the FCT evaluation. The FCT was performed in open air and consisted of an 1120 °C furnace hold for 60 min, followed by forced air cooling to 100 °C within 10 min. All TBC samples were tested in one single batch. The samples were monitored for surface integrity using an automated image capture system of the sample stage on cooling. TBC failure was deemed to have occurred when 20% of the TBC surface showed spallation. The TBCs for FCT were sprayed onto puck-shaped (25.4 mm diameter × 6.2 mm thick) Hastelloy X substrates. The substrates were previously grit-blasted with white Al_2O_3. The BC was 150-200 μm thick, and the YSZ topcoat was 400-450 μm thick. Both layers were sprayed using the 3MB APS torch, as previously described.

An industrial reference TBC was also added to the FCT study to serve as a control. The industrial reference TBC was sprayed using another commercial APS torch (F4-MB, Oerlikon Metco, Westbury, NY, USA) via an Ar-H_2 plasma. Both BC and YSZ topcoat were sprayed using the F4-MB APS torch. The reference YSZ feedstock was a conventional commercially available A&S powder with a comparable particle size distribution to AuerCoat YSZ LD-A. The industrial reference TBC was sprayed at the powder feed rate of 90 g/min and exhibited an average deposition rate of ∼ 10 μm/pass (high robot motion speed). Moreover, the industrial reference YSZ ceramic topcoat exhibited thickness comparable to those of the 3MB APS torch samples (∼ 400 μm). The porosity of the YSZ TBC reference was approximately 15%.

Results and Discussion

TBC Engineering Using Ar-H_2 and N$_2$-H_2 Plasmas

Figure 2 shows the resulting particle temperature (Tp) and particle velocity (Vp) values for the YSZ TBCs produced via the spray parameters described in Table 3. It is assumed a standard deviation (SD) of ± 5% for the Tp and Vp values. It is evident that the Ar-H_2 plasmas yielded lower Tp and higher Vp values than those yielded by N$_2$/H_2 plasmas, as generally observed by Marple et al. (Ref 4). It is important to stress that the SD of 7.5 cm was the same for all spray sets. Consequently, the higher Tp values observed for the N$_2$-H_2 plasmas were highly related to

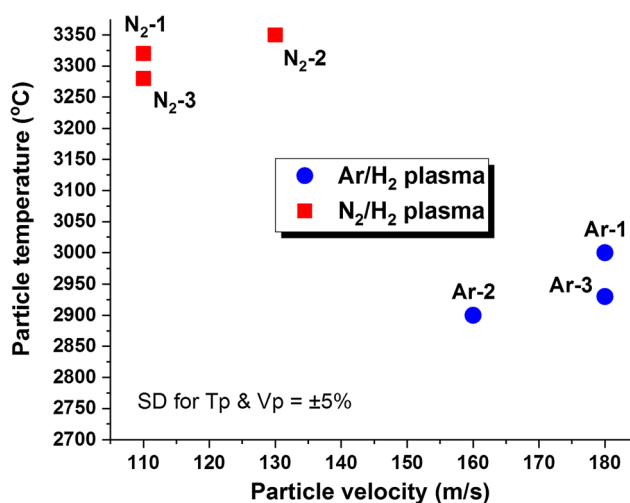increased dwell time of those particles in the plasma plume (lower Vp levels).

TBC As-Sprayed Microstructures

The cross-sectional as-sprayed TBC microstructures observed by SEM are given in Fig. 3 and 4. All YSZ TBCs are well-adhered to the BC (absence of horizontal gaps), and no vertical or horizontal cracks are found. However, it is noticed that the YSZ TBCs sprayed via N$_2$-H$_2$ plasmas (Fig. 4) are denser than those sprayed using Ar-H$_2$ plasmas (Fig. 3).

Deposition Efficiency Values

The deposition rate (DR) and DE values for each set of spray parameters are summarized in Table 4. It is possible to observe that the YSZ DE values reached over 50% only when the N$_2$-H$_2$ plasma was employed. It needs to be stressed that the higher DR and DE values of the N$_2$-H$_2$ YSZ TBCs did not cause unwanted defects on the coatings (i.e., debonding and/or delamination).

Phase Composition via XRD

The XRD patterns of the YSZ feedstock powder and as-sprayed coatings are given in Fig. 5. Briefly, no amorphous phases were detected and all XRD patterns were matched to their respective powder diffraction files (PDFs). The YSZ powder feedstock exhibited a combination of monoclinic (PDF #37-1484) and (PDF #82-1245) tetragonal phases. All as-sprayed Ar-H$_2$ YSZ TBCs exhibited the tetragonal t'-phase (PDF #48-0224) as the major phase and a minor percentage of monoclinic phase (PDF #37-1484),
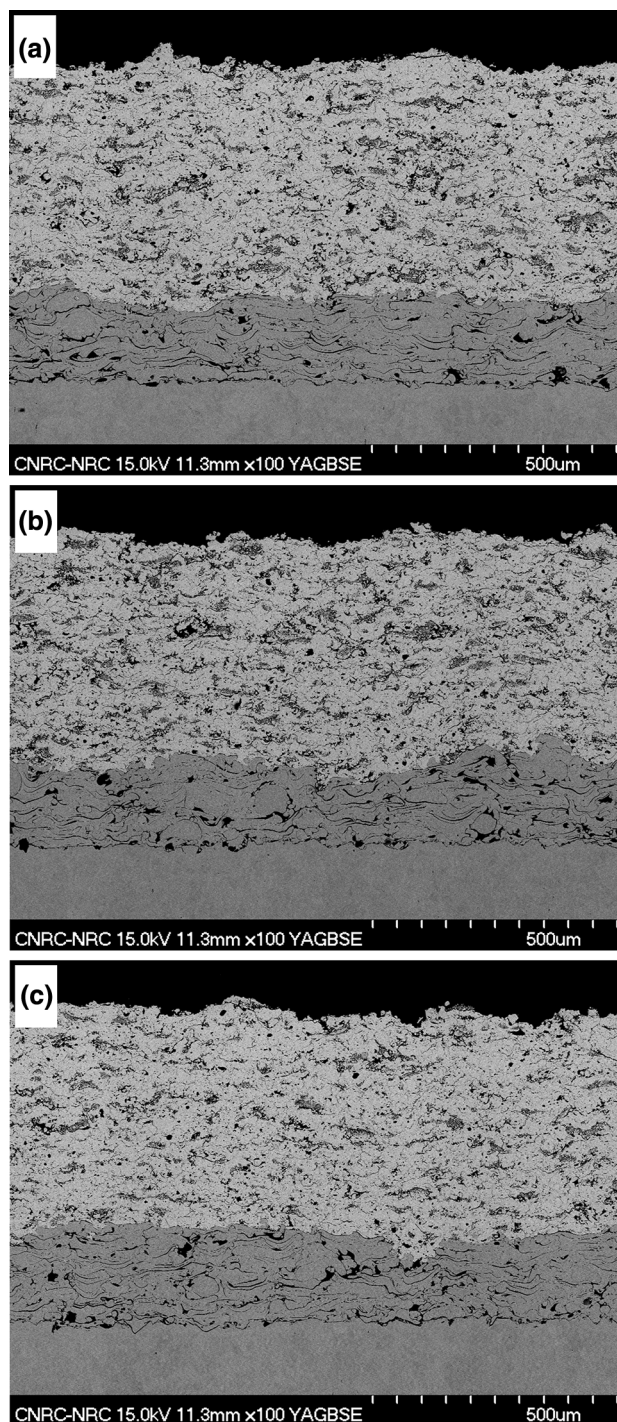

Fig. 3 Ar-H$_2$ as-sprayed TBC microstructures—(a) Ar-1, (b) Ar-2, and (c) Ar-3

identified in the low-intensity peaks at 2Θ values of $\sim$ 28° and $\sim$ 31°. All as-sprayed N$_2$-H$_2$ YSZ TBCs exhibited only the tetragonal t'-phase (PDF #48-0224).

Toraya et al. (Ref 10) made a calibration curve for the quantification of the monoclinic-tetragonal ZrO$_2$ system:
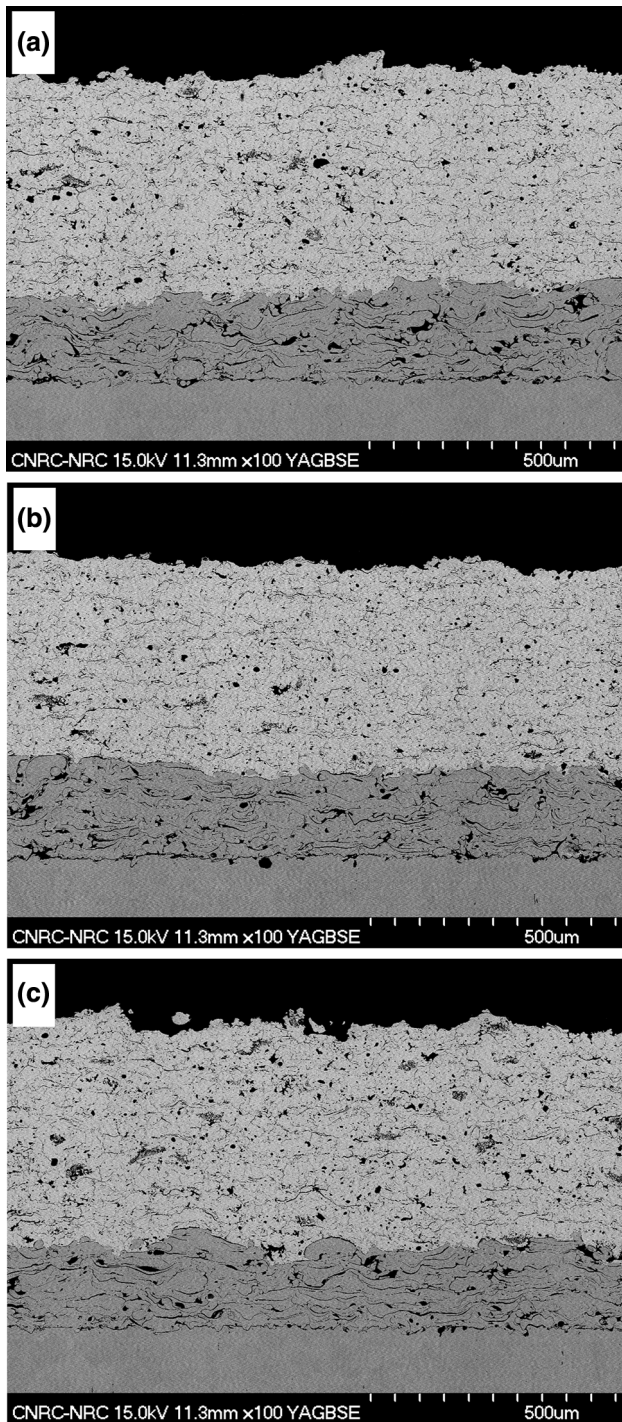
Fig. 4 N$_2$-H$_2$ as-sprayed TBC microstructures—(a) N$_2$-1, (b) N$_2$-2, and (c) N$_2$-3

$$V_m = \frac{1.311 X_m}{1 + 0.311 X_m}$$

$$X_m = \frac{I_m(\bar{1}11) + I_m(111)}{I_m(\bar{1}11) + I_m(111) + I_t(101)}$$

Table 4 Summary of the YSZ DR and DE values for the Ar/H$_2$ and N$_2$/H$_2$ plasmas

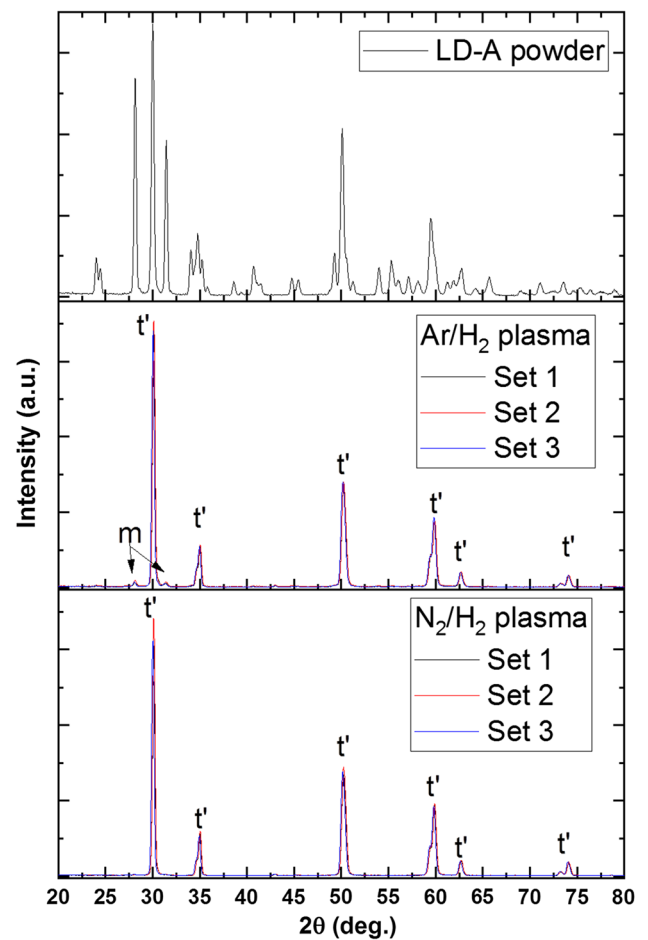| Set	Plasma	DR, μm/pass	DE, %
Ar-1	Ar/H$_2$	$\sim$ 31	36
Ar-2	Ar/H$_2$	$\sim$ 23	30
Ar-3	Ar/H$_2$	$\sim$ 29	38
N$_2$-1	N$_2$/H$_2$	$\sim$ 44	62
N$_2$-2	N$_2$/H$_2$	$\sim$ 43	61
N$_2$-3	N$_2$/H$_2$	$\sim$ 43	60

Fig. 5 XRD patterns of the YSZ feedstock powder and as-sprayed coatings

where V_m is the volume fraction of the monoclinic phase, X_m is the integrated intensity ratio (area under the peak), and I_m and I_t are the integrated intensity ratios for the monoclinic and tetragonal phases, respectively. Based on this calibration (Ref 10), the V_m values for the YSZ feedstock powder, as well as, for the Ar-1, Ar-2, and Ar-3 YSZ TBCs were 61%, 4%, 5%, and 4%; respectively.

The high average particle temperatures generated during plasma spraying (Fig. 2) for the Ar-H_2 (2900-3000 °C) and N_2-H_2 (3280-3350 °C) plasmas provided enough thermal energy to switch the monoclinic phase into the tetragonal one. The minor percentage (4-5 vol.%) of the monoclinic phase on the Ar-H_2 YSZ TBCs was probably related to few residual unmolten particles that were embedded in the coating microstructure (i.e., lower temperature levels than those of the N_2-H_2-sprayed YSZ). Consequently, no significant difference of phase composition was observed when YSZ was sprayed via Ar-H_2 and N_2-H_2 plasmas, based on the spray conditions described in Tables 2 and 3.

Thermal Conductivity

The relationship between the TC values at room temperature (RT) and porosity for the as-sprayed YSZ TBCs is given in Fig. 6. The average porosity values for the Ar-H_2 and N_2-H_2 YSZ TBCs are found within the ranges of 20-22 and 13-15%, respectively. According to Kulkarni et al. (Ref 11), the TC values of as-sprayed YSZ TBCs deposited via the 3MB APS torch (using Ar-H_2 plasma) are found within in the range of $\sim$ 0.6-1.0 W/mK. As shown in Fig. 6, all three as-sprayed Ar-H_2 YSZ TBCs produced in this study exhibited average TC values varying from 0.75 to 0.85 W/mK. Two of the three N_2/H_2 YSZ TBCs exhibited TC values above the Ar-H_2 range, i.e., > 0.85 W/mK. However, the data also show that it is possible to produce YSZ TBCs using a N_2-H_2 plasma (e.g., N_2-3) that exhibit as-sprayed TC values within the range of those of Ar-H_2 YSZ TBCs (i.e.; 0.75-0.85 W/mK). In fact, Tan et al. (Ref 12) have also shown that YSZ TBCs sprayed using a N_2-H_2 plasma can also exhibit as-sprayed TC

values within the $\sim$ 0.6-1.0 W/mK range of the Ar-H_2 YSZ TBCs.

It is not the objective of this work to study and explain in detail why a denser YSZ TBC (e.g., N_2-3—porosity $\sim$ 15%—Fig. 5) can exhibit TC values in the range of those of more porous ones (e.g., Ar-1, Ar-2, and Ar-3—porosity $\sim$ 20-22%—Fig. 6). It is known that the higher the porosity, the lower the TC values of bulk ceramics. According to Carter and Norton (Ref 13), the TC of the air is 0.026 W/mK, a value which is significantly lower than those of the majority of ceramic oxides. Consequently, ceramics having higher porosity values will inherently exhibit lower TC values. However, another factor comes into play for determining TC in APS ceramic coatings. McPherson (Ref 14) highlighted that the true area of contact between two adjacent as-sprayed splats is about 20%, whereas the remaining 80% of the contact area is characterized by planar gaps of about 100 nm in thickness. Yet according to McPherson (Ref 15), the known "low" TC values of APS ceramic coatings can be explained in terms of a model not only involving the regular coating porosity but also involving the limited regions of contact between splats. This is the reason why as-sprayed ceramic APS coatings typically exhibit lower TC values than those of bulk materials, even when both exhibit similar levels of coarse porosity ($\sim$ 1-20 μm pore size). Corroborating to McPherson (Ref 14, 15), Kulkarni et al. (Ref 11) have also shown that the TC values of APS YSZ TBCs are highly influenced by the number of splat interfaces (boundaries) per coating thickness. Each single-splat boundary acts as a barrier impeding the heat transfer to the adjacent splat along the TBC thickness. Therefore, depending on the "ratio or compromise" between the amount of coarse pores and the number of splat boundaries, TBCs that are "denser" can exhibit similar TC values of those that are "more porous" (Ref 11). Based on the DR and DE data of Table 4 and the porosity data of Fig. 6, it can be hypothesized that the N_2-H_2 YSZ splats were probably thinner than the Ar-H_2 ones. Consequently, if this is correct, the number of splat interfaces per YSZ thickness of the N_2-H_2 TBCs is higher than those of the Ar-H_2 TBCs. For this reason, it is thought that the N_2-H_2 TBC N_2-3 reached the "optimal" pore/splat-interface ratio, thereby being "denser" but still exhibiting "low" TC values. Nonetheless, Table 4 also shows that the DR values for all 3 N_2-H_2 YSZ TBCs were similar ($\sim$ 43-44 μm/pass), although the N_2-3 coating was slight more porous than the other two N_2-H_2 YSZ TBCs (Fig. 6). For this reason, it can be stated that understanding the fundamentals of the thermal conductivity behavior of thermal spray ceramic coatings is a complex task.

Although these initial results are promising, one may ask what would happen to the TC values after the TBCs are exposed to high temperatures. One may hypothesize that
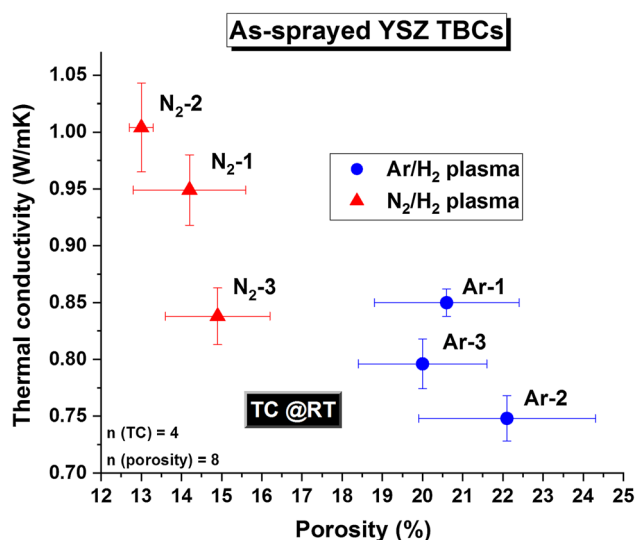

Fig. 6 Thermal conductivity at RT versus porosity values for as-sprayed YSZ TBCs produced using Ar-H_2 and N_2-H_2 plasmas

the TC values of the N$_2$-H$_2$ YSZ TBCs would significantly surpass those of the Ar-H$_2$ YSZ TBCs, which would render any practical applications of these N$_2$-based TBCs unrealistic. In order to address this issue, one group of YSZ TBCs was initially heat-treated in air at 1200 °C for 10 h, whereas a second group was heat-treated in air at 1400 °C for 20 h. The heat treatments were employed to cause an initial sintering and aging of the samples. They also guarantee that the YSZ microstructures would remain nearly stable prior to TC measurements at high temperatures (i.e., 1200 °C).

The TC results for the heat-treated YSZ TBCs (1200 °C-10 h) measured from RT to 1200 °C are shown in Fig. 7. It is possible to observe that the average TC values at 1200 °C for all Ar-H$_2$ YSZ TBCs are found within the range of 0.85-1.0 W/mK. Nonetheless, the average TC value for the N$_2$-H$_2$ N$_2$-3 YSZ TBC is also found in this range. In fact, from RT to 1200 °C, the average TC values of the N$_2$-3 YSZ TBC were always within the range of the Ar-H$_2$ YSZ TBCs (Fig. 7).

The TC results for the heat-treated YSZ TBCs (1400 °C-20 h) measured from RT to 1200 °C are shown in Fig. 8. It needs to be stressed that the heat treatment at 1400 °C for 20 h was done with the purpose of over-sintering and over-aging the samples. It helps considerably to answer the question about the TC stability of N$_2$-H$_2$ YSZ TBCs at high temperatures. It is possible to observe that the average TC values at 1200 °C for all Ar-H$_2$ YSZ TBCs are found within the range of 1.0-1.3 W/mK. Nonetheless, the average TC value for the N$_2$-H$_2$ N$_2$-3 YSZ TBC is also found in this range. Here again, from RT to 1200 °C, the

average TC values of the N$_2$-3 YSZ TBC were always within the range of the Ar-H$_2$ YSZ TBCs (Fig. 8).

Evidently, the lowest YSZ TC values in all conditions tested in this study were always provided by the Ar-H$_2$ TBC set Ar-2. However, as stated in "Rationale and Objectives" section, the objective of this study was not to produce a "better" coating, but rather produce a TBC that (1) falls within the current spec range and (2) that simultaneously exhibits significantly higher DE levels. Therefore, these results (Fig. 6, 7, 8) show that N$_2$-H$_2$ YSZ TBCs can be engineered to exhibit TC values within those of the Ar-H$_2$ YSZ TBCs from RT to high temperatures.

By looking into Fig. 7 and 8 in more detail, as expected due to the heat treatment, all TC values at RT are found above 1.0 W/mK. It is also possible to notice that all TC values maintained a steady nearly linear decrease from RT to 600 °C at a similar slope. However, after 800 °C, the TC values continue their steady nearly linear decrease, but at a lower rate, i.e., the slope changed and became "less steep". These changes in slopes are related to the different contributions of heat transfer mechanisms to TC.

Heat transfer occurs via conduction, radiation, and convection. As ceramic materials like YSZ do not exhibit free electrons, the conduction is caused by a vibration of an array of atoms (i.e., lattice wave or phonons). The phonons can be imagined as behaving like sound waves. As the temperature increases, the scattering and interference of the adjacent waves (phonons) are so high that they tend to cancel each other, thereby causing the TC values to decrease. This is likely what occurred with the TC values from RT to 600 °C (Fig. 7, 8). However, at 800 °C and
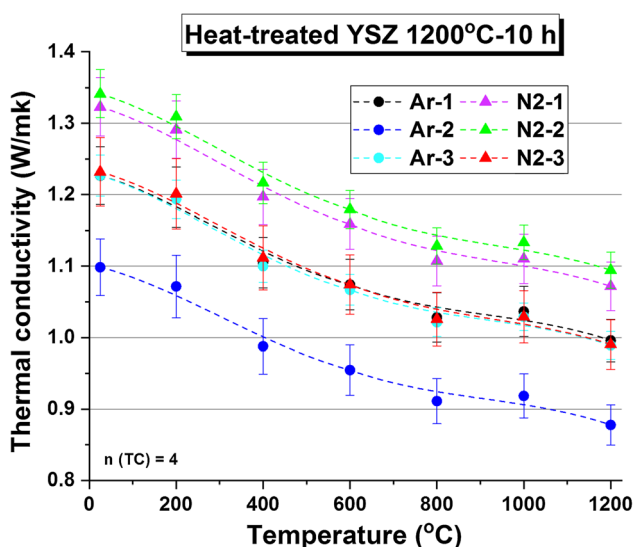

Fig. 7 Thermal conductivity versus temperature for heat-treated (1200 °C-10 h) YSZ TBCs produced using Ar-H$_2$ and N$_2$-H$_2$ plasmas
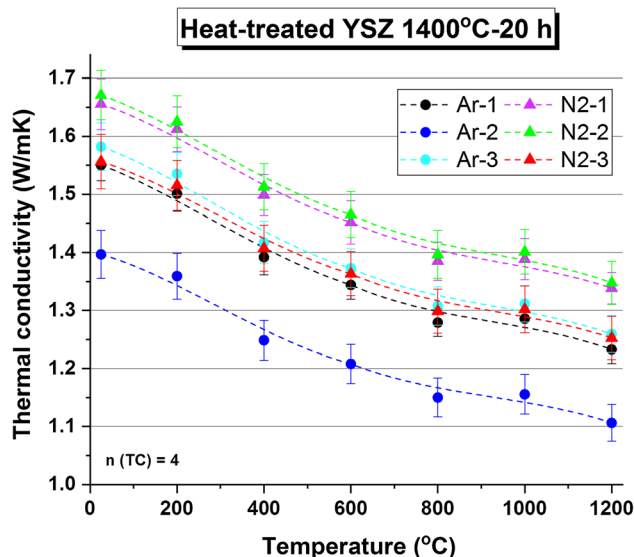
Fig. 8 Thermal conductivity versus temperature for heat-treated (1400 °C-20 h) YSZ TBCs produced using Ar-H$_2$ and N$_2$-H$_2$ plasmas

higher temperatures, the radiant heat transfer becomes more predominant. In radiation, heat is transferred via infrared (IR) electromagnetic waves ($\sim$ 1-1000 μm). At this IR wavelength range, ceramics can be transparent to the radiation and heat can be transported through the ceramic material. Consequently, the heat transfer efficiency and TC likely began to increase at 800 °C and higher temperatures, as shown in Fig. 7 and 8. This is probably what caused the change of the TC versus temperature slope observed at and after 800 °C (Fig. 7, 8). This radiation contribution effect causing an increase in TC values at high temperatures (above 800 °C) for APS YSZ TBCs has also been reported by Tan et al. (Ref 12). Regarding convection, the effect is considered to be minor for APS TBCs. In convention, the heat is transferred by the motion of a gas or fluid. Ratzer-Scheibe and Schulz (Ref 16) measured the TC values of as-sprayed and heat-treated (1100 °C-100 h) APS YSZ TBCs from RT to 1100 °C. The TC values were measured in vacuum and in argon gas atmosphere. It was concluded that the presence of the argon gas in the pores of a TBC increased the TC values of an average of roughly $\sim$ 10% (compared to vacuum), from RT to 1100 °C.

Thermal Cycle Life Performance via FCT

It is important to highlight again that "conventional wisdom" would claim that N_2-H_2 plasma YSZ TBCs would be "too dense," thereby yielding (1) high stiffness, (2) low capability to accommodate stress/strain, and (3) low performance in thermal cycle life. Consequently, performing an FCT study is paramount to test this hypothesis. The number of cycles to failure for the Ar-H_2, N_2-H_2, and industrial reference APS YSZ TBCs is shown in Fig. 9. The DE values for the Ar-H_2 and N_2-H_2 TBCs were also included to better compare and understand the overall TBC performance. Briefly, the APS YSZ TBCs Ar-2 and N_2-3 exhibited the highest and nearly equivalent FCT lifetimes ($\sim$ 370 cycles). This performance means an average improvement of 75% in lifetime when compared to the industrial reference APS YSZ TBC ($\sim$ 210 cycles). Moreover, the N_2-3 TBC exhibited a 100% DE improvement when compared to the Ar-2 TBC. In addition, it is important to point out at the best N_2-H_2 FCT-performing TBC (N_2-3) also exhibited RT and high-temperature TC values within those of all Ar-H_2 TBC produced in this study (Fig. 6, 7, 8).

Therefore, the results of Fig. 6, 7, 8 and 9 show that N_2-H_2 YSZ TBCs can be engineered to (1) exhibit thermal cycle performance levels similar to those of Ar-H_2 YSZ TBCs, (2) at the same time exhibiting twice the DE values, and (3) TC values within the range of those of Ar-H_2 YSZ TBCs.
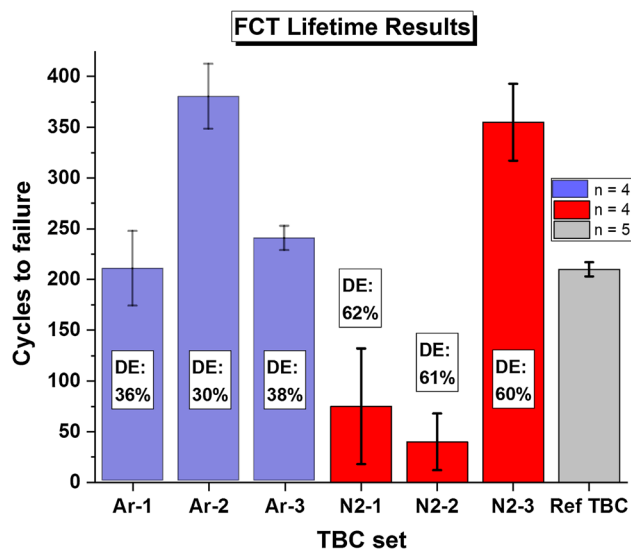

Fig. 9 Number of cycles to failure and DE values for different sets of APS YSZ TBCs

Considerations on FCT Performance

It is well beyond the scope of this work to investigate in detail the differences in FCT performance and failure mechanisms of the TBCs tested in this study. However, the data gathered during this study provided some trends. Initially, it is important to state that the generic APS YSZ TBC failure mechanisms during thermal cycling are relatively well-known and were summarized by Padture et al. (Ref 17).

The key aspect in TBC spallation failure is the formation of the ceramic-based thermally grown oxide (TGO) layer at the metallic bond coat during high-temperature exposure. The TGO is typically Al_2O_3-based, with the possible addition of other oxides coming from the other MCrAlY BC metals. The TGO can reach up to $\sim$ 10 microns at the spallation of the YSZ topcoat. During the cooling stage of a turbine engine (e.g., shutoff), the mismatch between the coefficient of thermal expansion (CTE) of the Al_2O_3-based TGO ($\sim 7 \times 10^{-6}$/K) and the metallic-based BC ($\sim 14 \times 10^{-6}$/K) results in high compressive residual stresses in the TGO. These thermal stresses reach a maximum at RT. Besides, the thicker the TGO, the higher the stress/strain in the system will be (Ref 17).

As the TGO thickens during high-temperature exposure, it keeps "jacking up" the YSZ topcoat during the ongoing cooling cycles. The TBC spallation onset of the YSZ topcoat starts in the form of a network of randomly dispersed horizontally oriented microcracks, which are formed when the stress/strain energy generated during cooling surpasses the fracture toughness of the TBC. These microcracks begin to propagate horizontally upon further cycles until they coalesce and form a major larger crack,

thereby leading to the macroscopic spallation of the YSZ topcoat (Ref 17). The horizontally oriented microcracking typically propagates within four distinct zones, such as (1) at the YSZ/TGO interface, (2) at the TGO/BC interface, (3) within the TGO, or (4) within the YSZ topcoat but adjacent to the TGO.

As previously stated, the failure of TBCs in thermal cycling (e.g., FCT) is driven by the oxidation of the BC at high temperatures. Consequently, it is accepted that the lower the BC oxidation rate, the longer the TBC life. In the case of this work, as stated in "TBC Production using Ar-H_2 and N_2-H_2 Plasmas" section, all Ar-H_2 and N_2-H_2 YSZ TBCs were sprayed on the same identical BC. Consequently, the differences in the performances of the Ar-H_2 and N_2-H_2 APS YSZ TBCs as shown in Fig. 9 are likely to be attributed to the ability of the YSZ topcoat structures to resist the stress of thermal cycling, as well as the stresses generated due to the growth of the TGO. This issue will be discussed in the next paragraphs of this section.

Figure 10 and 11 show the after FCT failure microstructural pictures of all six Ar-H_2 and N_2-H_2 APS YSZ TBCs, in which the FCT results are depicted in Fig. 9. It is possible to notice that the Ar-H_2 and N_2-H_2 APS YSZ TBCs tend to fail in distinct ways. By looking at the Ar-H_2 TBCs (Fig. 10), the spallation crack failure mainly occurred at the YSZ/TGO interface. On the other hand, the spallation crack failure mainly occurred within the YSZ topcoat but adjacent to the TGO for the N_2-H_2 TBCs (Fig. 12).

As a comparison, the microstructures of the as-sprayed and after FCT failure industrial reference APS Ar-H_2 YSZ TBC (F4 legacy APS torch) are shown in Fig. 12. The as-sprayed industrial reference TBC exhibits the typical porous and microstructural characteristics of a standard APS TBC (Fig. 12a). The TBC is well attached to the substrate and no major horizontal or vertical cracks are observed. Regarding the industrial reference TBC after FCT failure (Fig. 12b), the spallation crack failure for the reference TBC mainly occurred at the YSZ/TGO interface, like the Ar-H_2 TBCs produced for this study.

By looking at Table 4, one can see that the average deposition rate for the N_2-H_2 TBCs was $\sim$ 43-44 μm/pass, whereas that of the Ar-H_2 TBCs was $\sim$ 23-31 μm/pass. Regarding the N_2-H_2 TBCs after FCT failure, the spallation crack is approximately located $\sim$ 40-50 μm above the TGO (Fig. 11), i.e., at the thickness of the very first series of YSZ passes. Therefore, it is hypothesized that the higher deposition rates for the N_2-H_2 TBCs likely have generated higher residual stress levels when compared to those of the Ar-H_2 TBCs. Concomitantly, it is also hypothesized that these higher residual stress levels led to a failure within the YSZ topcoat but adjacent to the TGO. In addition, the higher porosity levels of Ar-H_2 TBCs (Fig. 6) and their
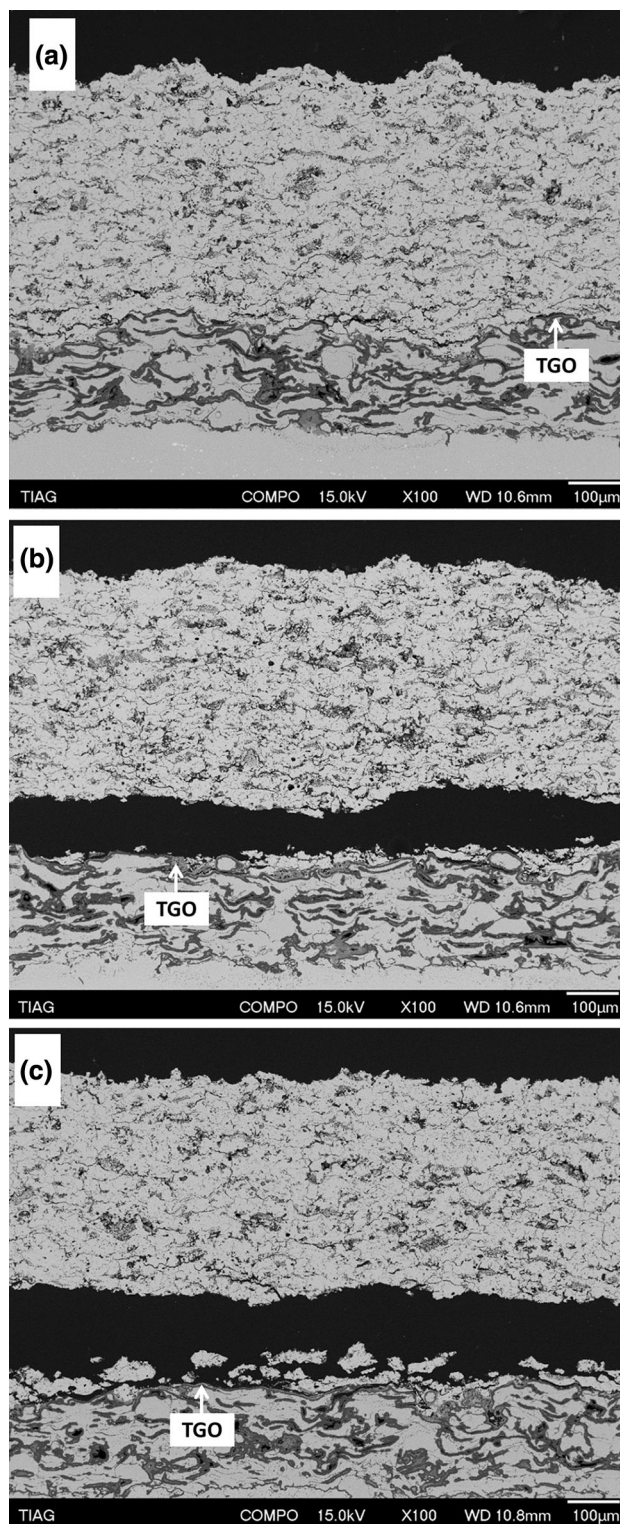

Fig. 10 Ar-H_2 TBC microstructures after FCT failure—(a) Ar-1 ($\sim$ 200 cycles), (b) Ar-2 ($\sim$ 350 cycles) and (c) Ar-3 ($\sim$ 230 cycles)

lower DR and DE values (Table 4) should further allow them greater tolerance for stress. It needs to be remembered that the industrial reference TBC was sprayed at an
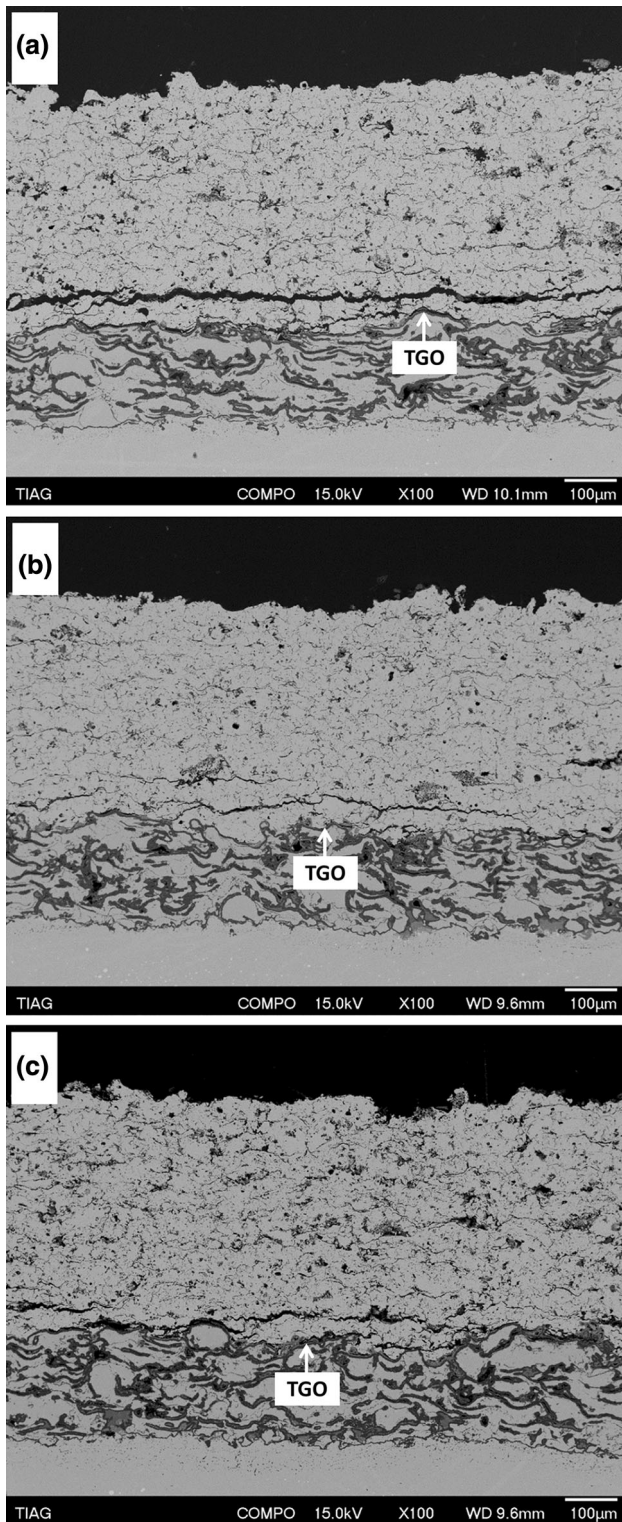
Fig. 11 N_2-H_2 TBC microstructures after FCT failure—(a) N_2-1 ($\sim$ 50 cycles), (b) N_2-2 ($\sim$ 25 cycles) and (c) N_2-3 ($\sim$ 350 cycles)
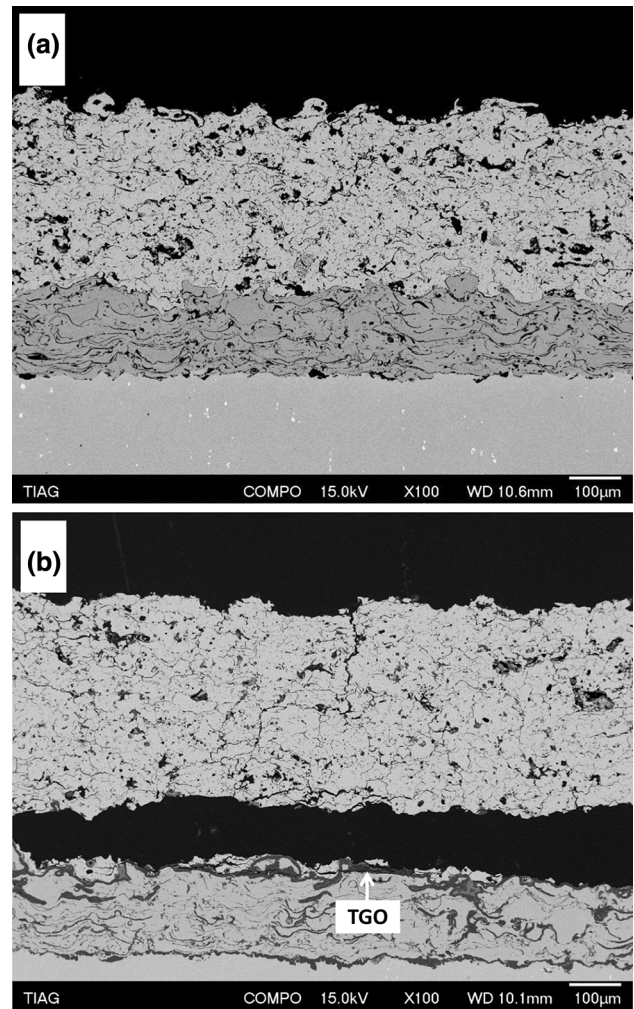

Fig. 12 Industrial reference Ar-H_2 APS YSZ TBC—(a) as-sprayed and (b) after FCT failure ($\sim$ 210 cycles)

Ar-H_2 TBCs tested in this work (i.e., industrial reference included) spalled and failed at the same coating region.

In order to try to pinpoint the differences in FCT performance, other trends related to the TBC failure during FCT evaluation need to be taken into account. Table 5 shows the APS torch power levels employed to spray the TBCs, as well as, the E values of the as-sprayed and after FCT failure YSZ TBCs and the number of cycles to failure in FCT. It is evident that within each TBC group (Ar-H_2 versus N_2-H_2), the TBCs sprayed with the lowest plasma power exhibited the longer FCT life. It is thought that lower plasma power levels most probably induced lower residual stress levels in the TBCs, which could lead to an improved performance in thermal cycling.

It is observed that the best Ar-H_2 (Ar-2) and N_2-H_2 (N_2-3) FCT-performing TBCs exhibit the lowest E values after FCT failure. Roughly, the E value is a measure of the stiffness of a material. Therefore, materials that exhibit "low" E values will be "less stiff" and more compliant to

average deposition rate of $\sim$ 10 µm/pass, which should limit the generation of residual stress levels. Therefore, all

Table 5 Elastic modulus (E) values measured via IIT of as-sprayed and after FCT failure YSZ TBCs—the indentations were performed on the cross-sections of the samples—plasma torch power and number to FCT cycles to failure also included

Set	E, GPa 300 gf As-sprayed YSZ (n = 10-12)	E, GPa 300 gf After FCT failure YSZ (n = 10-12)	Plasma torch power, kW	#Cycles FCT (n = 4)
Ar-1	90 ± 10	88 ± 8	38	210 ± 37
Ar-2	85 ± 9	76 ± 8	36	380 ± 32
Ar-3	96 ± 8	90 ± 11	39	240 ± 12
N_2-1	119 ± 3	122 ± 8	33	75 ± 57
N_2-2	111 ± 3	125 ± 8	37	40 ± 28
N_2-3	115 ± 5	117 ± 8	29	355 ± 38

tolerate stress/strain situations, such as those that occur in thermal cycling. According to Kingery et al. (Ref [18]), under a thermal cycling, the stress (σ) generated under a brittle ceramic material will be directly proportional to the E value of the material, its CTE (α) value and the temperature variation (ΔT); i.e., $\sigma = - E\alpha (T_{final} - T_{initial})$. As all TBCs exhibited the same CTE and were subjected to the same average ΔT, the lower E values after FCT failure of the Ar-2 and N_2-3 TBCs in their respective groups may have played a role in regarding their "good performances" in FCT.

Finally, it is known that the presence of the monoclinic phase can induce stresses in the YSZ TBCs during thermal cycling. By looking at the YSZ phase diagram reported by Muraleedharan et al. (Ref [19]), this is related to the volumetric changes associated with the monoclinic-to-tetragonal phase transformation upon heating (> 600 °C) and to the subsequent tetragonal-to-monoclinic phase transformation upon cooling (< 600 °C). According to VanValzah and Eaton (Ref [20]), the volumetric changes of the tetragonal-to-monoclinic transformation upon cooling are within the range 2.7-4.2%, i.e., there is an increase in material volume during this phase transformation. As previously stated, the failure of the TBCs occurs during the cooling process. For this reason, the presence of the monoclinic phase in YSZ TBCs is undesirable. The volumetric expansion related to the phase transformation would increase even more the stress/strain levels generated by the TGO and likely contribute to an earlier TBC spallation. Based on the XRD patterns of Fig. 5, no monoclinic phase was observed for the N_2-H_2 YSZ TBCs. A minor presence of the monoclinic phase (4-5 vol.%) was detected for as-sprayed the Ar-H_2 YSZ TBCs. However, based on the FCT performance of the TBCs (Fig. 9), it is unlikely that the minor monoclinic phase created a major negative effect on the performance of the Ar-H_2 YSZ TBCs. It is assumed that earlier Ar-H_2 YSZ TBC spallation failures would occur if it was the case.

Environmental Footprint, Economical Aspects, and Ar-H_2 versus N_2-H_2 Plasma Cost Production Estimation

In the twenty-first century, companies need to adapt more than ever to stiffer competition, society awareness, and tougher environmental laws. To stay ahead of the competition, the industry needs to increase its productivity at the same time decrease its environmental footprint, i.e., the amount of natural resources and energy they use. With this concept in mind, the percentage reduction in overall cost and time for TBC production when an Ar-H_2 plasma is replaced by a N_2-H_2 one was estimated. The two most performing TBCs, regarding lowest TC values (Fig. 6, 7, 8) and highest FCT lifetime (Fig. 9), were chosen for the estimation, i.e., Ar-2 and N_2-3.

The estimation was based on the spraying a 400-450-μm-thick YSZ TBC on a 500-mm-long cylindrical component. This part could be considered as being similar to the inner wall of an annular turbine combustion chamber. The component tangential speed, the torch transverse speed, powder feed rate, DR and DE values used to estimate the cost, and time to deposit the TBC were the ones used and obtained for this study. The cost of the consumables and energy were: 30 US\$/m^3 for Ar, 22 US\$/m^3 for N_2, 38 US\$/m^3 for H_2, and 34 US\$/kg for YSZ feedstock, and 0.25 kWh for electricity. Other costs involved (e.g., labor) were not included in the estimation.

The Ar-H_2 versus N_2-H_2 plasma cost production estimation is summarized in Table 6. Briefly, by changing from an Ar-H_2 plasma to a N_2-H_2 one, there is a reduction of (1) 47% in YSZ feedstock consumption, (2) 58% in electricity consumption, (3) 47% in processing time, and (4) 55% in total overall coast. As previously stated, reducing environmental footprint means reducing at the same time the amount of natural resources and energy used to produce a product. Consequently, the data of Table 6 unequivocally show the important environmental and

Table 6 Estimation of the consumption of consumables/electricity/electricity/time and the percentage reduction in cost and time when replacing the Ar-H₂ Ar-2 by the N₂-H₂ N₂-3 plasma set (400-450 μm YSZ TBC—500-mm-long cylinder)

Consumption	Ar/H₂ (Ar-2)	N₂/H₂ (N₂-3)	N₂/H₂ reduction, %
Primary Ar	7.92 m³	n.a.	− 61
	US$237.50		
Primary N₂	n.a.	4.17 m³	
		US$91.67	
Secondary H₂	1.58 m³	0.83 m³	− 47
	US$60.17	US$31.67	
YSZ feedstock	3483.33 g	1833.33 g	− 47
	US$118.43	US$62.33	
Electricity	US$23.75	US$10.07	− 58
Time	158.3 min	83.3 min	− 47
Total cost	US$439.85	US$195.74	− 55

n.a.—not applicable

economic benefits of using N₂-H₂ plasmas in legacy APS torches for TBC production.

Final Considerations

Although these initial results are promising, further development and testing must be done in order to qualify for production N₂-H₂ YSZ TBCs deposited via legacy APS torches. One of the typical concerns of using N₂-H₂ plasmas is the erosion and longevity of the electrodes, i.e., cathode and nozzle (anode). An early erosion of the nozzle could introduce unacceptable variations in the TBC microstructure, as well as contamination of electrode materials (e.g., via Cu spiting) in the TBC itself.

However, the electrode set lifetime depends on different factors, which includes (Ref 21): (1) plasma torch power levels, (2) plasma torch cooling water quality, (3) average run time between plasma torch starts and stops, (4) plasma process gases used, (5) plasma process gases purity, (6) spray processing tolerances, (7) the use of W-lined Cu nozzles, (8) the use of original or generic torch electrode sets, and (9) how the plasma torch is turned on and off (i.e., smooth or sudden ramp). For these reasons, it is known the electrode set lifetime is very difficult to predict, and it can vary a lot from booth to booth, even within the same facility and/or institution. According to the manufacturer of the W-lined Th-free Cu nozzles, its employment provides two to three times the nozzle life and reduces torch maintenance (Ref 21).

What can be stated at this moment is the fact that for this R&D (1) original equipment manufacturer (i.e., not generic) Th-free cathodes and W-lined Th-free Cu nozzles

were employed, (2) the Ar-H₂ plasma electrode set was 1.2 h old when the R&D started, (3) the N₂-H₂ plasma electrode set was 13.6 h old when the R&D started, (4) tap water was employed as plasma torch cooling water, (5) the plasma torch is turned on & off in a smooth ramp, and (6) the Ar, N₂, and H₂ plasma gases purity levels were 99.998, 99.998, and 99.99%; respectively.

Besides torch electrode lifetime issues, TBC erosion, burner-rig testing, among others, will need to be investigated in detail in order to approve these coatings on the different turbine original engine manufacturers (OEM) specs.

Conclusions

A commercial YSZ feedstock was sprayed using a legacy APS torch. Two types of plasmas were employed: Ar-H₂ and N₂-H₂. Although Ar-H₂ and N₂-H₂ spray parameters yielded significantly different values of particle T&V, no major differences in phase composition were observed for the as-sprayed coatings. Regarding FCT performance, the best-performing Ar-H₂ and N₂-H₂ YSZ TBCs exhibited nearly equivalent thermal cycle lifetimes (FCT). In addition, the best FCT-performing N₂-H₂ YSZ TBC exhibited a 100% improvement in deposition efficiency when compared to the best FCT-performing Ar-H₂ TBC (i.e., 60% versus 30%). The RT and high-temperature thermal conductivity values of the best FCT-performing N₂-H₂ YSZ TBC (set N₂-3) were in the range of those of all Ar-H₂ YSZ TBCs produced during this study (sets Ar-1, Ar-2, and Ar-3). These initial results show that under optimized spray conditions, N₂-H₂ YSZ TBCs have the potential to simultaneously (1) minimize production costs, (2) increase productivity, (3) reduce environmental footprint, and (4) meet Ar-H₂ YSZ TBC specs. Based on the improved thermal spray processing quality control available in the twenty-first century (e.g., Industry 4.0), it is thought that this R&D should be continued and the Ar-H₂ versus N₂-H₂ plasma comparison needs to be revisited.

References

1. A. Feuerstein, J. Knapp, T. Taylor, A. Ashary, A. Bolcavage, and N. Hitchman, Technical and Economical Aspects of Current Thermal Barrier Coating Systems for Gas Turbine Engines by

Thermal Spray and EBPVD: A Review, *Journal of Thermal Spray Technology*, 2008, **17**(2), p 199-213

2. H.S. Ingham, Jr, and A.J. Fabel, Comparison of Plasma Flame Spray Gases, *Welding Journal*, 1975, **10**, p 101-105

3. A.B. Murphy and C.J. Arundell, Transport Coefficients of Argon, Nitrogen, Oxygen, Argon-Nitrogen, and Argon-Oxygen Plasmas, *Plasma Chemistry and Plasma Processing*, 1994, **14**(4), p 451-490

4. B.R. Marple, R.S. Lima, C. Moreau, S.E. Kruger, L. Xie, and M.R. Dorfman, Yttria-Stabilized Zirconia Thermal Barriers Sprayed Using N_2-H_2 and Ar-H_2 Plasmas: Influence of Processing and Heat Treatment on Coating Properties, *Journal of Thermal Spray Technology*, 2007, **16**(5–6), p 791-797

5. A. El-Zein, M. Talaat, G. El-Aragi, and A. El-Amawy, Electrical Characteristics of Nonthermal Gliding Arc Discharge Reactor in Argon and Nitrogen Gases, *IEEE Transactions on Plasma Science*, 2016, **44**(7), p 1155-1159

6. S. Sampath, U. Schulz, M.O. Jarligo, and S. Kuroda, Processing Science of Advanced Thermal-Barrier Systems, *MRS Bulletin*, 2012, **37**(7), p 903-910

7. W.C. Oliver and G.M. Pharr, Measurement of Hardness and Elastic Modulus by Instrumented Indentation: Advances in Understanding and Refinements to Methodology, *Journal of Materials Research*, 2004, **19**(1), p 3-20

8. G. Di Girolamo, C. Blasi, L. Pagnotta, and M. Schoppa, Phase Evolution and Thermophysical Properties of Plasma Sprayed Thick Zirconia Coatings after Annealing, *Ceramics International*, 2010, **36**, p 2273-2280

9. R.E. Taylor, X. Wang, and X. Xu, Thermophysical Properties of Thermal Barrier Coatings, *Surface and Coatings Technology*, 1999, **120–121**, p 89-95

10. H. Toraya, M. Yoshimura, and S. Somita, Quantitative Analysis of Monoclinic-Stabilized Cubic ZrO_2 Systems by X-Ray Diffraction, *Journal of the American Ceramic Society*, 1984, **67**(9), p C-183–C-184

11. A. Kulkarni, Z. Wang, T. Nakamura, S. Sampath, A. Goland, H. Herman, J. Allen, J. Ilavsky, G. Long, J. Frahm, and R.W. Steinbrech, Comprehensive Microstructural Characterization and Predictive Property Modeling of Plasma-sprayed Zirconia Coatings, *Acta Materialia*, 2003, **51**, p 2457-2475

12. Y. Tan, J.P. Longtin, S. Sampath, and H. Wang, Effect of the Starting Microstructure on the Thermal Properties of As-sprayed and Thermally Exposed Plasma-Sprayed YSZ Coatings, *Journal of the American Ceramic Society*, 2009, **92**(3), p 710-716

13. C. Barrycarter and M. Grantnorton, *Ceramic Materials: Science and Engineering*, Springer, New York, 2007, p 626-627

14. R. McPherson, A Review of Microstructure and Properties of Plasma Sprayed Ceramic Coatings, *Surface and Coatings Technology*, 1989, **39**(40), p 173-181

15. R. McPherson, A Model for the Thermal Conductivity of Plasma-Sprayed Ceramic Coatings, *Thin Solid Films*, 1984, **112**, p 89-95

16. H.-J. Ratzer-Scheibe and U. Schulz, The Effects of Heat Treatment and Gas Atmosphere on the Thermal Conductivity of APS and EB-PVD PYSZ Thermal Barrier Coatings, *Surface and Coatings Technology*, 2007, **201**, p 7880-7888

17. N.P. Padture, M. Gell, and E.H. Jordan, Thermal Barrier Coatings for Gas-Turbine Engine Applications, *Science*, 2002, **296**, p 280-284

18. W.D. Kingery, H.K. Bowen, and D.R. Uhlmann, *Introduction to Ceramics*, 2nd ed., Wiley, New York, 1976, p 816-817

19. K. Muraleedharan, J. Subrahmanyam, and S.B. Bhaduri, Identification of t' Phase in ZrO_2-7.5 wt.%Y_2O_3 Thermal-Barrier Coatings, *Journal of the American Ceramic Society*, 1988, **71**(5), p C-226–C-227

20. J.R. VanValzah and H.E. Eaton, Cooling Rate Effects on the Tetragonal to Monoclinic Phase Transformation in Aged Plasma-Sprayed Yttria Partially Stabilized Zirconia, *Surface and Coatings Technology*, 1991, **46**, p 289-300

21. https://www.oerlikon.com/ecomaXL/files/metco/oerlikon_SF-0013.1_3MB_9MB_W-Nozzles_EN.pdf&download=1. Accessed 12 Oct 2018